WATER RESOURCES RESEARCH, VOL. 49, 7126–7132, doi:10.1002/wrcr.20501, 2013

High-resolution fracture aperture mapping using optical profilometry

Pasha Ameli,[1] Jean E. Elkhoury,[1] and Russell L. Detwiler[1]

Received 8 May 2013; revised 19 August 2013; accepted 24 August 2013; published 2 October 2013.

[1] Fractures play an important role in the Earth's crust, often controlling both mechanical and transport processes. Developing a mechanistic understanding of these processes requires quantifying the roughness of fracture surfaces and the contacts and void spaces between fracture surfaces at high spatial resolution (10s of microns) over a broad range of scales (centimeters to meters). Here we present a scalable method for measuring fracture surfaces and reconstructing fracture aperture fields using an optical profilometer. We evaluate the method by measuring two fractured limestone cores; one is a tensile fracture with strong cross correlation between the surfaces and the other is a saw-cut, sand-blasted fracture with negligible cross correlation between the surfaces. Results of repeated measurements of these two fractures suggest that well-correlated surfaces, where the correlation between the surfaces can aid reconstruction, can be reproduced with local uncertainties with median standard deviation of 8 μm. Poorly correlated surfaces, where reconstruction relies solely upon the precision of the placement of the halves of the core on the profilometer stage, can be reproduced with local uncertainties with median standard deviation of 20 μm. Additionally, we quantified the accuracy of the technique by comparing calculated aperture profiles of a fractured concrete core to thin sections cut from the core after impregnating it with epoxy. The median deviation between the two measurements, which includes errors due to residual misalignment of the profiles, was 29 μm supporting the accuracy of the method. Our results emphasize the potential for using noncontact surface measurement techniques to accurately and precisely reconstruct fracture apertures over a wide range of length scales.

Citation: Ameli, P., J. E. Elkhoury, and R. L. Detwiler (2013), High-resolution fracture aperture mapping using optical profilometry, *Water Resour. Res.*, *49*, 7126–7132, doi:10.1002/wrcr.20501.

1. Introduction

[2] Fractures play an important role in the mechanical and transport properties of rock formations. Fracture-surface roughness influences both fracture stiffness and resistance to shear [*Bandis et al*., 1983], which in turn influence the onset of seismic events [*Renard et al*., 2012] and the propagation of seismic waves [*Liu*, 2005]. Shearing of fracture or fault surfaces subsequently affects surface roughness [*Candela et al*., 2012]. The geometry of the void space between contacting rough fracture surfaces (fracture aperture) controls fluid flow and transport processes through rock formations [*Berkowitz*, 2002]. This has led to numerous efforts to characterize these fundamental properties of fractured rock over the past several decades ranging from field measurements at kilometer scales to laboratory measurements in centimeter-scale cores [*Renard et al*., 2006; *Candela et al*., 2012]. Laboratory-scale measurements are often combined with flow [*Schmittbuhl et al*., 2008] and transport experiments [*Durham et al*., 2001] or deformation experiments [*Nemoto et al*., 2009] to clarify the role of fracture geometry on these processes. A fundamental challenge with these efforts lies in resolving small-scale features that may control the processes being observed (10s of microns or smaller) over scales that are large enough to include a representative range of heterogeneity (centimeters or greater).

[3] Early efforts to measure fractures involved destructive techniques such as injecting epoxy and then slicing the rock perpendicular to the fracture to make direct measurements of fracture profiles [e.g., *Hakami and Larsson*, 1996]. This technique can provide accurate characterization of fracture roughness, but the resolution in one direction is limited to the thickness of the rock slices. Furthermore, destructive evaluation is not well suited to experiments aimed at quantifying how mechanical or chemical processes alter fracture properties. Nondestructive methods for studying the role of fracture geometry on different mechanisms include a range of energy absorption techniques: X-ray computed tomgraphy (CT) [*Montemagno and Pyrak-Nolte*, 1995; *Noiriel et al*., 2013], magnetic resonance imaging (MRI) [*Baraka-Lokmane et al*., 2001; *Becker et al*., 2003], and transmitted light in transparent analog fractures [*Detwiler et al*., 1999; *Isakov et al*., 2001]. Light transmission techniques are ideally suited to detailed, quantitative

[1]Department of Civil and Environmental Engineering, University of California, Irvine, California, USA.

Corresponding author: R. L. Detwiler, Department of Civil and Environmental Engineering, University of California, Irvine, CA 92697-2175, USA. (detwiler@uci.edu)

0043-1397/13/10.1002/wrcr.20501

observations of fundamental mechanisms in well-controlled geometries [*Detwiler*, 2010], but these are simplifications of real rock fractures. MRI provides the ability to directly measure both fracture geometry and fluid motion through fractures. However, limited spatial resolution requires propping fractures open to create millimeter-scale fracture apertures [*Dijk et al*., 1999; *Becker et al*., 2003].

[4] X-ray CT can provide micrometer-scale measurements of fracture geometry, and potentially pore geometry and mineral distribution within the rock matrix with spatial resolution directly related to the size of the sample. *Ketcham et al*. [2010] suggest a practical limit of voxel sizes limited to about 1/1000 of the sample size. This is a particularly significant limitation when studying processes in fractures, which typically exhibit high aspect ratios with apertures of 10–100 μm and areal extents of 10–100 cm or larger. Furthermore, we are typically interested in the void space between fracture surfaces, which comprises a very small fraction of the total volume included in the three-dimensional reconstruction of a fractured core. Significant processing of data sets consisting of O (10^9) voxels is thus required to extract quantitative information about fracture geometry.

[5] Surface profilometers provide an alternative approach for nondestructively characterizing fracture surface topography. Profilometers typically measure the displacement of a stylus contacting the rock surface at discrete locations [*Durham and Bonner*, 1993] or measure the distance to the surface from a fixed reference elevation using optical techniques [*Brown*, 1987]. Challenges with contact profilometry are the relatively slow acquisition rate ($\sim$0.1 Hz) and the potential for surface damage caused by the contacting stylus. Optical profilometry techniques require no contact with the surface and have acquisition rates that are orders of magnitude faster and, thus, provide the potential to overcome the size limitations inherent with X-ray CT methods. Currently available optical profilometers are capable of micron-scale resolution of surface elevations on grids with spatial resolution as high as $\sim$10 μm. Such measurements provide quantitative insights into the roughness characteristics of fracture surfaces, in the form of a two-dimensional array of surface elevations, resulting in more compact data sets than those obtained with X-ray CT at similar resolution. However, relating surface elevations to fracture apertures remains a challenge [*Schmittbuhl et al*., 2008].

[6] Different reconstruction techniques have been used to quantify aperture fields in efforts to: (i) relate fracture surface roughness to fracture aperture [*Brown*, 1995; *Lanaro*, 2000]; (ii) quantify characteristics of fractures that intercept boreholes [*Tatone and Grasselli*, 2012; *Neuville et al*., 2012]; and (iii) understand how surface roughness may influence the hydraulic [*Durham and Bonner*, 1994] and mechanical [*Brown and Scholz*, 1986; *Sharifzadeh et al*., 2008] properties of fractures. In addition, these reconstruction techniques provide the potential to quantify changes in fracture aperture induced by mechanical and chemical processes [*Durham et al*., 2001; *Yasuhara et al*., 2006; *Elkhoury et al*., 2013]. However, interpreting the results from such experiments requires that aperture changes resulting from a specific experiment can be distinguished from measurement and reconstruction errors. This requires a systematic evaluation of measurement reproducibility, which, to our knowledge, has not been previously described.

[7] We present and evaluate a noncontacting method for measuring fracture surfaces and numerically combining them to determine the aperture between the surfaces. The approach relies upon a custom jig designed to register and secure samples during the measurement process and careful numerical reconstruction of the measured surfaces.

2. Measurement Method

[8] The process for quantifying fracture apertures using a surface profilometer involves two primary steps: (1) measuring fracture surface topography and (2) numerically mating the measured surfaces. We use an optical profilometer (Nanovea ST400) to measure surface topography on a regular grid over both fracture surfaces. The optical profilometer focuses a beam of white light on the fracture surface using a lens with a well-characterized axial chromatic aberration. The spectrum of the projected light is stretched in the axial direction such that the wavelength of the reflected light is directly correlated with the distance of the corresponding point on the surface to the lens. This measurement is less sensitive to variations in surface reflectivity than other optical profilometry methods such as white-light interferometry and laser profilometry.

[9] The sample is fixed to a stage mounted on an *x*-*y* linear positioning system that is actuated by precision stepping motors. A computer controls and coordinates the motion of the stage and data acquisition and records elevations with a measurement rate up to 1000 Hz. By selecting different lenses, one can adjust the vertical resolution of the measurements and the diameter of the spot of light reflecting from the surface. For the current study, we used a spot diameter of 8 μm and vertical measurement range of 3.5 mm. The profilometer used in this study can measure surfaces up to 15×15 cm at spatial resolutions as small as the spot diameter. We used a spatial resolution of 20×20 μm resulting in a maximum scanning rate of 2 cm/s.

[10] Fractures consist of two contacting rough rock surfaces resulting in distributed points of contact between the surfaces and regions of void space with variable aperture. We fabricated a jig to aid with registration and alignment of the two halves of fractured cores (Figure 1) and facilitate numerical reconstruction of fracture aperture fields. The jig consists of two mated steel blocks with sides polished to $\pm$12 μm of flat and square (Figure 1a). Four steel dowels fit into opposing tight-clearance holes to register the blocks (Figure 1b). A hole drilled along the intersection of the two blocks with a diameter $\sim$100 μm larger than the core diameter (3.81 cm for the samples used here) allows fastening the fractured core securely in the jig (Figure 1a). Prior to placing the halves of the core in the jig, we carefully mate the surfaces of the core and tape them together. Thin beads of silicone adhesive around each end of the core secure each half of the core to the jig and allow easy removal after scanning.

[11] After the adhesive cures, we remove the tape holding the halves together, open the jig and secure the halves side-by-side on the profilometer stage (Figure 1b). A precision dial gage aids accurate positioning of the two halves

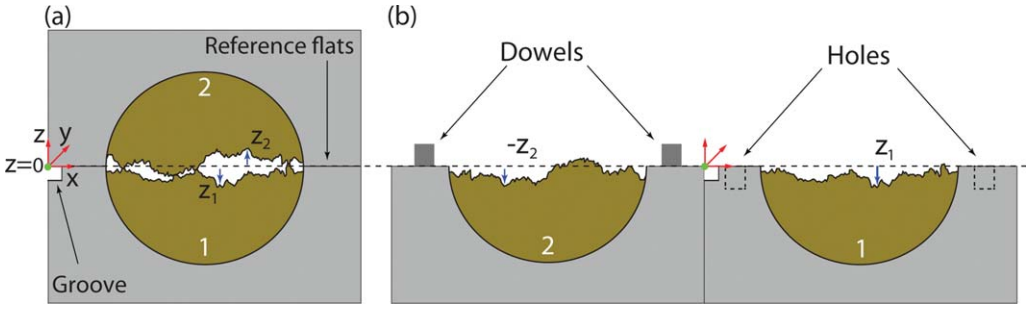

Figure 1. Schematic of a cross section of two halves of a core placed in the measurement jig (gray). (a) Adhesive secures the mated halves of the core inside the closed jig and (b) rotating the jig about the origin (green dot) exposes both surfaces for scanning. Local fracture aperture is defined as the sum of the distances, z_1 and z_2 from the reference surface ($z = 0$) defined by the reference flats. The notch removed from the jig holding surface 1 is a groove milled along the length of the jig and is used for locating $x = 0$ in each x direction scan. See Figure 4 in *Elkhoury et al*. [2013] for additional details.

of the jig on the profilometer stage such that the y axis of the jig is closely aligned ($\pm 12\,\mu$m) with the y axis of the profilometer stage. In addition, a shallow groove milled along the edge of one half of the jig provides a small step change in elevation along the axis of rotation of the jig (Figure 1a).

[12] The fracture surfaces of the two halves of the core can be represented at any point in the x-y plane as the distances $z_1(x,y)$ and $z_2(x,y)$ from the $z = 0$ datum, which is coplanar with the reference flats on either side of the fractured core (Figure 1a). The aperture between the fracture surfaces is then:

$$b(x,y) = z_2(x,y) - z_1(x,y) \tag{1}$$

[13] The challenge with this approach lies in obtaining measurements of both $z_1(x,y)$ and $z_2(x,y)$ at identical locations of the x-y plane (Figure 1a), because the fractured core must be opened to allow measurement of the two surfaces (Figure 1b).

[14] Scanning the entire surface, including both halves of the core and the adjacent flat surfaces of the jig, provides: (i) direct measurements of the elevation of the datum, $z(x,y) = 0$, which corresponds to the reference surfaces of the jig adjacent to each half of the fracture; (ii) the location of the y axis, which can be identified as a step change in elevation at the groove along the edge of one half of the jig; and (iii) measurements of the rock surfaces, $z_1(x - \Delta x, y)$ and $-z_2(-x + \Delta x, y)$ over each fracture surface, where Δx represents a potential offset of the measurements from the actual location of the y axis on the jig. Small values of Δx can lead to potentially significant errors due to misalignment of the mated surfaces. Depending on the mode of fracture and the characteristics of the rock, fracture surfaces exhibit different degrees of cross correlation. Surfaces that are strongly cross-correlated provide a means of directly evaluating the alignment process and potentially correcting any associated errors. On the other hand, fracture surfaces that exhibit no cross correlation provide a worst-case scenario because the numerical mating of the surfaces depends solely on the relative alignment of the fracture halves within the jig, with no possibility of further adjustment.

[15] We demonstrate the measurement technique and evaluate resulting errors for both strongly and poorly cross-correlated surfaces by measuring two different limestone cores. One core was fractured using a Brazil test to create a well-mated tensile fracture (TF). To minimize damage to the edges of the core during fracturing, we fractured a 5.1 cm core and then removed a 3.8 cm subcore parallel to the fracture. We sawed the other core along its axis and sand blasted the surface of each half of the core to create rough surfaces (SC). Figure 3 shows measurements of the surfaces of one half of each core and the corresponding reconstructed fracture apertures.

[16] The small-scale variability of both fractures is similar, but, at spatial scales larger than about 1 mm, fracture SC exhibits no autocorrelation, whereas fracture TF exhibits a scale-invariant correlation structure. The reconstructed fracture apertures also exhibit very different characteristics, which are evident in Figure 3 and histograms of the fracture aperture fields (Figure 2a). The surfaces of fracture TF are strongly cross-correlated and as a result much of the fracture exhibits near-zero aperture. The localized regions of large aperture resulted from damage to the fracture surfaces during the fracturing process. The surfaces of fracture SC

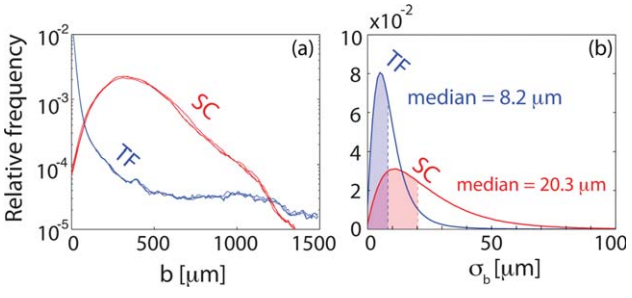

Figure 2. (a) Histograms of the three repeated measurements of fracture aperture, b, for both fractures are very similar. Histograms of the local standard deviation of the measured aperture, $\sigma_b(x,y)$, quantify local measurement uncertainty. The larger median value of $\sigma_b(x,y)$ for fracture SC reflects our inability to refine the registration of the two surfaces using cross correlation between the two surfaces (unlike fracture TF).

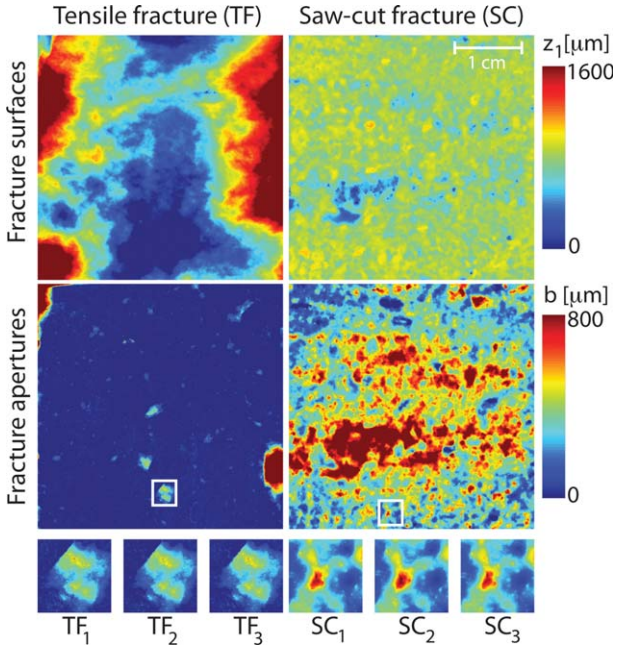

Figure 3. Measurements of the surface elevation of surface 1, z_1, for the tensile fracture (TF) and (top row) saw-cut fracture (SC) and (middle row) the corresponding reconstructed aperture fields, b. The large-aperture regions in TF correspond to regions where pieces of rock broke from the surface during fracturing, whereas the large aperture region in SC corresponds to a vug intersected by he fracture. The white boxes in both of the aperture fields highlight the region of interest (ROI) shown at larger scale for the three repeated measurements in the bottom row.

exhibit negligible cross correlation resulting in significant regions with nonzero fracture aperture and infrequent (relative to fracture TF) regions of contact. These two different fractures provide the opportunity to quantitatively explore the different sources of error in the aperture measurement process.

3. Evaluation of Errors

[17] Errors in the calculated values of $b(x,y)$ reflect a combination of: (i) measurement errors and (ii) reconstruction errors that result from the required numerical manipulation of measured values of $z_1(x,y)$ and $-z_2(-x,y)$. Here we discuss the details of these two fundamental sources of error and assess the cumulative effect on the final estimates of $b(x,y)$.

3.1. Measurement Errors

[18] There are two primary sources of error influencing the accuracy and precision of surface-elevation measurements. The first involves errors associated with quantifying the wavelength of the spot projected on the rock surface and converting it to an elevation at a specified position on the surface. This point-measurement error corresponds to the measurement uncertainty reported by the manufacturer ($\pm 1\ \mu$m for the optics used in this study). We verified precision of $<1\ \mu$m by repeatedly measuring the same location on a relatively flat surface. During these measurements, monitored room temperatures fluctuated by a maximum of $\pm 2°$C with no measurable correlation between measured elevations at a single point and temperature.

[19] The second involves random errors in the x-y position, $\vec{\varepsilon}(x,y)$, which cause the instrument to report an elevation at (x,y) when the actual location of the measurement corresponds to position $(x \pm \varepsilon_x, y \pm \varepsilon_y)$. These positional errors lead to additional measurement errors:

$$\varepsilon_z(x,y) = \vec{\varepsilon}(x,y) \cdot \vec{\nabla} z(x,y) \tag{2}$$

[20] For rock surfaces, $\vec{\nabla} z(x,y) \neq 0$, resulting in the potential for non-negligible values of $\varepsilon_z(x,y)$. We quantified $\varepsilon_z(x,y)$ by repeating the measurement of one of the surfaces for each fracture without moving the surface. Thus, discrepancies between the two measurements reflect a combination of point-measurement uncertainty and $\varepsilon_z(x,y)$. Furthermore, assuming ε_x and ε_y are zero-mean-independent random variables, squaring both sides of (2), and taking the expected value (represented by $\langle\rangle$) yields:

$$\langle \varepsilon^2 \rangle = \langle \varepsilon_z^2 \rangle \left[\left\langle \left(\frac{\partial z}{\partial x} \right)^2 \right\rangle + \left\langle \left(\frac{\partial z}{\partial y} \right)^2 \right\rangle \right]^{-1} \tag{3}$$

for $\langle \varepsilon^2 \rangle = \langle \varepsilon_x^2 \rangle \cong \langle \varepsilon_y^2 \rangle$. Applying this analysis to repeated scans of surfaces from fractures TF and SC as well as single profiles measured independently along the x and y directions yields estimates of $|\varepsilon_x|$ and $|\varepsilon_y|$ between 8 and 10 μm (less than half the spatial resolution of the measurements).

3.2. Reconstruction Errors

[21] Fracture-aperture reconstruction from measured surfaces involves three steps: (i) assess the alignment of the y axis of the jig with the y axis of the stage motion and adjust if necessary; (ii) determine the elevation of the $z(x,y) = 0$ plane shown in Figure 1 and remove it from the measured elevations of each surface; and (iii) transform the measurements of $-z_2(-x,y)$ to $z_2(x,y)$ and apply (1) to calculate $b(x,y)$. In addition, for the case of fracture surfaces exhibiting strong cross correlation, it is possible to check and, if needed, adjust the orientation of the surfaces by measuring cross correlation at local regions across the surfaces. We describe each of these processes and quantify the cumulative effect on the reproducibility of aperture measurements.

[22] The first reconstruction step is to align the jig with the y axis of the profilometer during scanning. The groove milled along the edge of one side of the jig (Figure 1) facilitates this process. Due to the 8 μm spot diameter and the 20 μm scanning resolution used here, the transition across the groove does not always result in a discrete jump. This allows subpixel-scale estimation of the location of the y axis on the scanned surfaces. Such deviations are below the resolution of the dial gage used to position the jig on the profilometer stage, but contribute to errors in reconstructing the fracture aperture caused by small misalignments between the z_1 and z_2 surfaces. We correct any observed deviations of the y axis by numerically rotating the scanned surfaces using a bilinear interpolation routine to approximate the surface elevations on the transformed grid. The result of this process is that the

measurement at (x,y) on surface 1 corresponds to the measurement at $(-x\pm\delta_x, y\pm\delta_y)$ on surface 2 (Figure 1), where δ_x and δ_y are residual alignment errors. At the 20-μm measurement resolution used in this study, the required rotation of the measured surfaces was less than 0.06°, corresponding to less than 40 μm over a length of 4 cm.

[23] Each half of the core can be adjusted to reflect the elevation difference from the $z(x,y) = 0$ datum by subtracting a plane fit to the flat surfaces on each half of the jig (Figure 1a). Applying (1) with these adjusted values of $z_1(x,y)$ and $z_2(x,y)$ yields the fracture aperture field, $b(x,y)$. Because the halves of the jig are always mated with each other before securing to the jig, the relative position of the two surfaces will be the same for repeated measurements, even if the absolute position of the core in the jig differs. Furthermore, by referencing each half of the core to the $z(x,y) = 0$ datum independently, it is not necessary for the reference surfaces on both halves of the jig to be coplanar. Thus, it is unnecessary for the jig to be perfectly square, but measurement accuracy does depend upon the flatness of the reference surfaces.

[24] We measured each core three times to assess the errors resulting from different steps within the reconstruction process. This process included removing the halves of the core from the jig after each measurement. We then mated the halves of the core again and secured them to the jig. Therefore, results include all potential sources of error and reflect the amount of variability one should expect when using this technique to measure fracture aperture before and after an experiment [*Elkhoury et al*., 2013].

[25] Because the fracture surfaces for fracture TF are strongly cross-correlated, we were able to check and improve the alignment of the fracture surfaces after initial processing. Cross-correlation matrices calculated over small regions of the surfaces provide local estimates of residual misalignment (δ_x, δ_y) between the surfaces that results from small discrepancies in the relative position of the halves of the core in the jig. For the measurements presented here, this process typically showed δ_x and δ_y to be less than 2 pixels (40 μm). Thus, fracture surfaces with poor cross correlation such that additional alignment corrections are not possible (e.g., fracture SC) will include errors due to potential ~40 μm misalignment of the fracture surfaces. The magnitude of errors resulting from misalignment will be larger for surfaces with larger root-mean-squared values of $\vec{\nabla} z(x,y)$ (i.e., greater short-wavelength roughness).

[26] Histograms of fracture aperture for the three repeated measurements of each core provide a fracture-scale quantitative measure of discrepancies in fracture aperture calculations (Figure 2a). The histograms exhibit very good agreement with well-reproduced fracture aperture statistics (e.g., mean, variance, skewness). In addition, direct quantitative comparison of local aperture measurements is also possible. This requires numerically aligning the measured aperture fields because the jig (Figure 1) was designed to facilitate only the relative alignment of the fracture surfaces, not the absolute location of the surfaces on the profilometer stage. We used the same process used for aligning the fracture surfaces of fracture TF to align repeated measurements of fracture aperture fields. We note that this may not always be possible for fracture measurements before and after an experiment if the entire fracture aperture field has been altered by the experiment. Such cases will require modifying the process presented here to ensure absolute registration of the fracture surfaces within the jig and the jig on the profilometer stage.

[27] Figure 3 shows regions of interest (white box outlined in large aperture fields) from the three measurements of fractures TF and SC. Differences between TF_1, TF_2, and TF_3 are difficult to detect visually, whereas differences between SC_1, SC_2, and SC_3 are more apparent (Figure 3). This reflects the relative magnitude of the error that results from using only the jig configuration (not cross correlation between surfaces) to align the fracture surfaces. The standard deviation of the aperture measurements, $\sigma_b(x,y)$, at each x,y provides a quantitative measure of the local uncertainty in fracture aperture measurements (Figure 2b). The median values of $\sigma_b(x,y)$ are 8.2 and 20.3 μm, for fractures TF and SC, respectively, with the difference reflecting the influence of the residual misalignment for fracture SC.

3.3. Fracture Aperture Accuracy

[28] The previous section focused on the precision of fracture aperture measurements. For experiments in which relative change in fracture aperture is of interest, measurement precision is critical. However, the accuracy of measurements is also important, though more difficult to quantify. To evaluate the accuracy of our approach, we fractured a well-cured concrete core (fractured using the same Brazil test method for fracture TF) and measured the aperture field using the technique described above. We then impregnated the core with epoxy and cut the core into a series of sections for optical imaging. Prior to injecting epoxy into the core, we imposed a 900 μm shear offset between the surfaces to create significant regions with nonzero aperture such that epoxy could readily flow through the fractured core.

[29] Because it is difficult to precisely cut sections that are located along the x- y coordinate system established by the profilometer, it is not possible to exactly collocate the measured profiles and the sawed sections. In an effort to overcome this challenge, we selected a set of scanned profiles from the vicinity ($\pm$200 μm) of each saw-cut section and selected the profile that best matched the saw-cut section (Figure 4a). Overlaying the profilometer reconstruction of the fracture profiles on the image of the saw-cut section of the epoxy-impregnated fractured core provides a useful qualitative comparison of the two methods (Figure 4a).

[30] Agreement between the measurement and actual surfaces is excellent over much of the profiles. Localized regions of disagreement (identified by arrows in Figure 4a) are likely due to misalignment of the saw-cut sections, either because of small misalignment in the y direction and possible small rotations (in the x-y plane) of the sections relative to the profiles, or to small errors in measured surface elevations. To test this hypothesis, we rotated the measured aperture field in an effort to better align the scanned profiles with the imaged slice. Figure 4b shows the result of this realignment process. The resulting profiles agree more closely with the measured profiles (Figure 4c). The corresponding aperture fields are also in excellent agreement (Figures 4d and 4e). To quantify the difference between the two aperture fields (Figure 4d), we report the distribution of minimum distances between the aperture

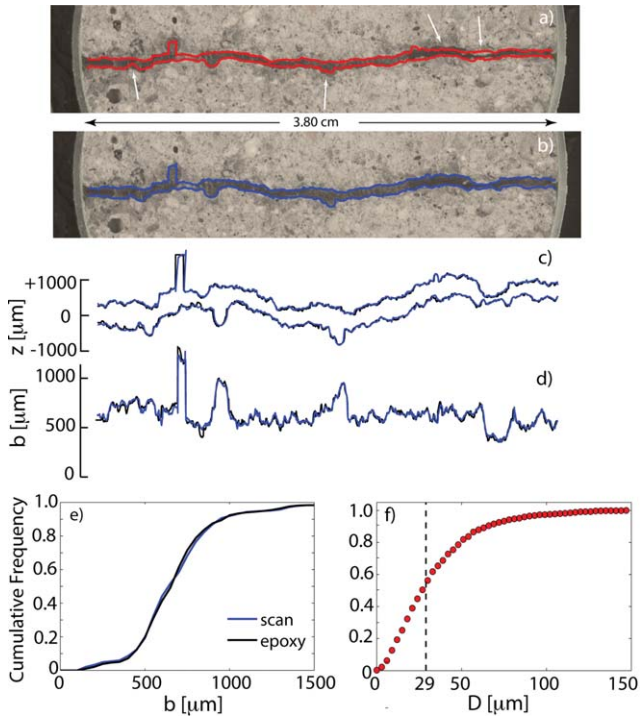

Figure 4. A typical example of a slice of the epoxy-filled, fractured, concrete core. The epoxy is the black region between the rock surfaces. (a) The red profiles are the nearest corresponding surface profiles measured with the profilometer and (b) the blue profiles show the same location with the scanned profiles rotated to better align with the imaged section. (c) The black profiles are direct digitizations of the fracture surfaces from the epoxy-filled fracture slice shown in Figures 4a and 4b. The fracture profiles and the aperture field in Figure 4d show excellent agreement between the measurements made with the profilometer and the imaged sections by (e) comparing the aperture distributions. To further quantify the difference between the two aperture profiles in Figure 4d, we measured the minimum distance, D, between the two profiles and plot (f) the cumulative distribution with median 29 μm.

fields obtained from the two methods (Figure 4f). The median value of 29 μm reflects the combination of residual alignment errors between the two measurement techniques and accuracy errors in the aperture-field reconstruction and supports the robustness of profilometer-based measurement of fracture apertures.

4. Conclusion

[31] We have presented a detailed analysis of an approach for using high-resolution fracture surface measurements to reconstruct fracture aperture fields. The approach combines a precision jig with white-light profilometry to accurately measure fracture surfaces and numerically reconstruct the fracture aperture field. We demonstrated the approach on two fundamentally different fractures: (1) a tensile fracture in a limestone core (TF) and (2) a saw-cut, sand-blasted limestone core (SC). Strong cross correlation between the surface of fracture TF facilitated careful alignment of the surfaces, whereas negligible cross correlation between the surfaces for fracture SC required reliance upon the measurement jig and the measurement process to align the fracture surfaces. Results suggest that surfaces can be reproduced with a median local standard deviation of 8 μm for well-correlated surfaces and 20 μm for uncorrelated surfaces.

[32] A potentially significant advantage of the approach presented here is the ability to quantify small-scale surface roughness and resulting aperture variability over relatively large scales. The profilometer used in the current study is capable of scanning surfaces up to 15 cm square, which provides the potential for cores with greater than 5 cm diameter. However, this approach is readily scalable. By reconfiguring the profilometer to move the measurement probe above the rock (rather than move the rock beneath the probe, which has practical limits in the ability of the stage to move a large mass of rock) the approach is only limited by the ability to accurately maintain the z position of the probe as it moves in the x and y directions. Thus, this approach has significant advantages over in situ measurement techniques such as X-ray CT where measurement scale and measurement resolution are implicitly linked.

[33] **Acknowledgment.** Funding for this research was provided by the U.S. Department of Energy, Office of Energy Sciences, Geosciences Program (contract DE-FG02–09ER16003).

References

Bandis, S., A. Lumsden, and N. Barton (1983), Fundamentals of rock joint deformation, *Int. J. Rock Mech. Min. Sci.*, *20*, 249–268.

Baraka-Lokmane, S., G. Teutsch, and I. G. Main (2001), Influence of open and sealed fractures on fluid flow and water saturation in sandstone cores using magnetic resonance imaging, *Geophys. J. Int.*, *147*, 263–271.

Becker, M. W., M. Pelc, R. V. Mazurchuk, and J. Spernyak (2003), Magnetic resonance imaging of dense and light non-aqueous phase liquid in a rock fracture, *Geophys. Res. Lett.*, *30*(12), 1646, doi:10.1029/2003GL017375.

Berkowitz, B. (2002), Characterizing flow and transport in fractured geological media: A review, *Adv. Water Resour.*, *25*, 861–884.

Brown, S. R. (1987), Fluid flow through rock joints: The effect of surface roughness, *J. Geophys. Res.*, *92*, 1337–1347.

Brown, S. R. (1995), Simple mathematical model of a rough fracture, *J. Geophys. Res.*, *100*, 5941–5952.

Brown, S. R., and C. H. Scholz (1986), Closure of rock joints, *J. Geophys. Res.*, *91*, 4939–4948.

Candela, T., F. Renard, Y. Klinger, K. Mair, J. Schmittbuhl, and E. E. Brodsky (2012), Roughness of fault surfaces over nine decades of length scales, *J. Geophys. Res.*, *117*, B08409, doi:10.1029/2011JB009041.

Detwiler, R., S. Pringle, and R. Glass (1999), Measurement of fracture aperture fields using transmitted light: An evaluation of measurement errors and their influence on simulations of flow and transport through a single fracture, *Water Resour. Res.*, *35*, 2605–2617.

Detwiler, R. L. (2010), Permeability alteration due to mineral dissolution in partially saturated fractures, *J. Geophys. Res.*, *115*, B09210, doi:10.1029/2009JB007206.

Dijk, P., B. Berkowitz, and P. Bendel (1999), Investigation of flow in water-saturated rock fractures using nuclear magnetic resonance imaging (NMRI), *Water Resour. Res.*, *35*, 347–360.

Durham, W., and B. Bonner (1993), Peak: A new kind of surface microscope, *Int. J. Rock Mech. Min. Sci.*, *30*, 699–702.

Durham, W. B., and B. P. Bonner (1994), Self-propping and fluid flow in slightly offset joints at high effective pressures, *J. Geophys. Res.*, *99*, 9391–9399.

Durham, W. B., W. L. Bourcier, and E. Burton (2001), Direct observation of reactive flow in a single fracture, *Water Resour. Res.*, *37*, 1–12.

Elkhoury, J. E., P. Ameli, and R. L. Detwiler (2013), Dissolution and deformation in fractured carbonates caused by flow of CO_2-rich brine under reservoir conditions, *Int. J. Greenhouse Gas Control*, *16S1*, S203–S215.

Hakami, E., and E. Larsson (1996), Aperture measurements and flow experiments on a single natural fracture, *Int. J. Rock Mech. Min. Sci.*, *33*, 395–404.

Isakov, E., S. R. Ogilvie, C. W. Taylor, and P. W. Glover (2001), Fluid flow through rough fractures in rocks I: High resolution aperture determinations, *Earth Planet. Sci. Lett.*, *191*, 267–282.

Ketcham, R. A., D. T. Slottke, and J. M. Sharp Jr. (2010), Three-dimensional measurement of fractures in heterogeneous materials using high-resolution X-ray computed tomography, *Geosphere*, *6*, 499–514.

Lanaro, F. (2000), A random field model for surface roughness and aperture of rock fractures, *Int. J. Rock Mech. Min. Sci.*, *37*, 1195–1210.

Liu, E. (2005), Effects of fracture aperture and roughness on hydraulic and mechanical properties of rocks: Implication of seismic characterization of fractured reservoirs, *J. Geophys. Eng.*, *2*, 38–47.

Montemagno, C., and L. J. Pyrak-Nolte (1995), Porosity of natural fracture networks, *Geophys. Res. Lett.*, *22*, 1397–1400.

Nemoto, K., N. Watanabe, N. Hirano, and N. Tsuchiya (2009), Direct measurement of contact area and stress dependence of anisotropic flow through rock fracture with heterogeneous aperture distribution, *Earth Planet. Sci. Lett.*, *281*, 81–87.

Neuville, A., R. Toussaint, and J. Schmittbuhl (2012), Fracture aperture reconstruction and determination of hydrological properties: A case study at draix (french alps), *Hydrol. Processes*, *26*, 2095–2105.

Noiriel, C., P. Gouze, and B. Made (2013), 3D analysis of geometry and flow changes in a limestone fracture during dissolution, *J. Hydrol.*, *486*, 211–223.

Renard, F., C. Voisin, D. Marsan, and J. Schmittbuhl (2006), High resolution 3D laser scanner measurements of a strike-slip fault quantify its morphological anisotropy at all scales, *Geophys. Res. Lett.*, *33*, L04305, doi:10.1029/2005GL025038.

Renard, F., K. Mair, and O. Gundersen (2012), Surface roughness evolution on experimentally simulated faults, *J. Struct. Geol.*, *45*, 99–110.

Schmittbuhl, J., A. Steyer, L. Jouniaux, and R. Toussaint (2008), Fracture morphology and viscous transport, *Int. J. Rock Mech. Min. Sci.*, *45*, 422–430.

Sharifzadeh, M., Y. Mitani, and T. Esaki (2008), Rock joint surfaces measurement and analysis of aperture distribution under different normal and shear loading using gis, *Rock Mech. Rock Eng.*, *41*, 299–323.

Tatone, B. S. A., and G. Grasselli (2012), Quantitative measurements of fracture aperture and directional roughness from rock cores, *Rock Mech. Rock Eng.*, *45*, 619–629.

Yasuhara, H., A. Polak, Y. Mitani, A. S. Grader, P. M. Halleck, and D. Elsworth (2006), Evolution of fracture permeability through fluid–rock reaction under hydrothermal conditions, *Earth Planet. Sci. Lett.*, *244*, 186–200.